Inorganic Chemistry

Article

pubs.acs.org/IC

Theoretical Investigation on Multiple Bonds in Terminal Actinide Nitride Complexes

Qun-Yan Wu,[†] Cong-Zhi Wang,[†] Jian-Hui Lan,[†] Cheng-Liang Xiao,[†] Xiang-Ke Wang,[‡] Yu-Liang Zhao,[†] Zhi-Fang Chai,*[,†,§] and Wei-Qun Shi*[,†]

[†]Key Laboratory of Nuclear Radiation and Nuclear Energy Technology, and Key Laboratory for Biomedical Effects of Nanomaterials and Nanosafety, Institute of High Energy Physics, Chinese Academy of Sciences, Beijing, 100049, China

[‡]Key Laboratory of Novel Thin Film Solar Cells, Institute of Plasma Physics, Chinese Academy of Sciences, Hefei, 230031, China

[§]School of Radiological and Interdisciplinary Sciences (RAD-X), and Collaborative Innovation Center of Radiation Medicine of Jiangsu Higher Education Institutions, Soochow University, Suzhou 215123, China

Supporting Information

ABSTRACT: A series of actinide (An) species of L-An-N compounds [An = Pa–Pu, L = $[N(CH_2CH_2NSiPr^i_3)_3]^{3-}$, $Pr^i = CH(CH_3)_2$] have been investigated using scalar relativistic density functional theory (DFT) without considering spin–orbit coupling effects. The ground state geometric and electronic structures and natural bond orbital (NBO) analysis of actinide compounds were studied systematically in neutral and anionic forms. It was found that with increasing actinide atomic number, the bond length of terminal multiple An–N1 bond decreases, in accordance with the actinide contraction. The Mayer bond order of An–N1 decreases gradually from An = Pa to Pu, which indicates a decrease in bond strength. The terminal multiple bond for L–An–N compounds contains one σ and two π molecular orbitals, and the contributions of the 6d orbital to covalency are larger in magnitude than the 5f orbital based on NBO analysis and topological analysis of electron density. This work may help in understanding of the bonding nature of An–N multiple bonds and elucidating the trends and electronic structure changes across the actinide series. It can also shed light on the construction of novel An–N multiple bonds.

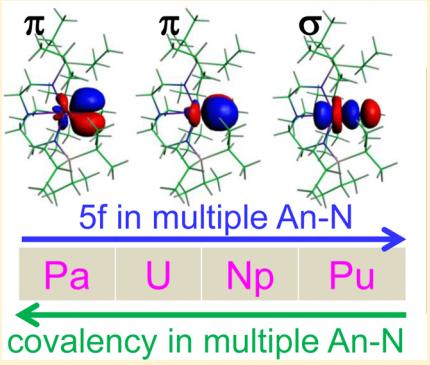

1. INTRODUCTION

Many complexes with multiple bonds are known for main group and transition metal elements,[1−4] such as carbon, nitrogen, oxygen, and metals. Actinide compounds with actinide-ligand multiple bonds are relatively rare compared to those of the main group elements.[5,6] Gilje et al. reported the first uranium carbene complex containing a uranium multiple bond with a ligand in 1981.[5] In recent years, complexes containing actinide-ligand multiple bonds have received widespread attention due to their unique structural properties and potential applications in synthesis and catalysis.[7−16] Such multiple bonds between actinide and main-group ligands, especially for terminal oxo, nitrido, imido, carbene ligands as well as chalcogens, are often observed for early actinides. For example, the CUO molecule was detected with laser ablation techniques and the U–C bond was found to possess quadruple bond character.[17,18] Bart and co-workers reported a complex $Tp^*_2U{=}O$ [Tp* = hydrotris(3,5-dimethylpyrazolyl)borate] with a U=O bond length of 1.863 Å.[19] Although many uranium nitride complexes have been synthesized, most of them feature a bridging binding mode. Liddle and co-workers first reported a terminal uranium(V) nitride and identified it to be a U–N triple bond of 1.825 Å in length in 2012.[13] Subsequently, they isolated the first uranium(VI) complex including a terminal uranium nitride triple bond of 1.799 Å (Scheme 1) through mild redox reactions.[15]

Scheme 1. Structures of L-U-N Compound and Ligand [L = $[N(CH_2CH_2NSiPr^i_3)_3]^{3-}$ and $Pr^i = CH(CH_3)_2$]

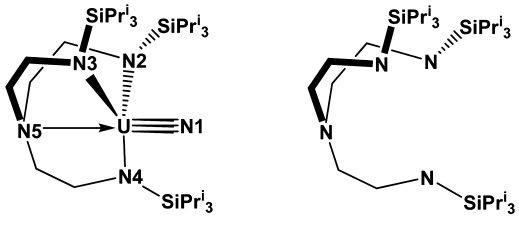

The observations of a terminal uranium nitride triple bond set a new benchmark for 5f orbital participation in bonding and opened the door for unprecedented actinide-mediated reactivity. However, multiple bonds across actinide series are not well explored compared to those of main elements and transition metals. At the same time, actinide analogues of other

Received: April 30, 2014
Published: September 3, 2014

   dx.doi.org/10.1021/ic501006p | Inorg. Chem. 2014, 53, 9607–9614

Table 1. Terminal U−N1 Bond Distances (R, Å) and the Corresponding Harmonic Vibrational Frequencies (ν, cm^{-1}) in Neutral and Anionic L-U-N Species at BP86, B3LYP, PBE, and M06-2X Methods with 6-31G(d) and 6-31+G(d) Basis Sets, Respectively[a]

species	parameter	expt	BP86	B3LYP	PBE	M06-2X
$[L\text{-}U\text{-}N]^-$	$R_{6\text{-}31G(d)}$	1.825(15)[b]	1.805(1.1%)	1.782(2.4%)	1.802(1.2%)	1.766(3.3%)
	$R_{6\text{-}31+G(d)}$	1.825(15)[b]	1.805(1.1%)	1.782(2.4%)	1.802(1.2%)	1.766(3.3%)
	$\nu_{6\text{-}31G(d)}$	936[b]	917(2.0%)	969(3.5%)	905(3.3%)	1001(6.9%)
	$\nu_{6\text{-}31+G(d)}$	936[b]	922(1.5%)	966(3.2%)	924(1.3%)	–[d]
L-U-N	$R_{6\text{-}31G(d)}$	1.799(7)[c]	1.773(1.4%)	1.743(3.1%)	1.770(1.6%)	1.709(5.0%)
	$R_{6\text{-}31+G(d)}$	1.799(7)[c]	1.773(1.4%)	1.743(3.1%)	1.770(1.6%)	1.709(5.0%)
	$\nu_{6\text{-}31G(d)}$	914[c]	938(2.6%)	1008(10.2%)	943(3.2%)	1099(20.2%)
	$\nu_{6\text{-}31+G(d)}$	914[c]	936(2.1%)	1006(9.7%)	942(2.7%)	1093(19.2)

[a]The values in parentheses are the relative errors compared to experimental results. [b]Ref 13. [c]Ref 15. [d]"–" denotes not available.

than the L-U-N compounds have not been explored experimentally or theoretically. Actually, all actinide compounds are radioactive and toxic, especially transuranic elements, which hinders experimental studies with them. Fortunately, at present quantum chemical studies can provide another useful approach to disclose the electronic structures and bonding natures of actinide compounds. Although there have been many reports about computational studies of actinide complexes,[17,20−31] few efforts focus on the covalency and bonding nature of multiple bonds.[18,32−35] Therefore, it is highly desirable to understand the trends and differences of 5f orbital participation in actinide-ligand multiple bonds across the actinide series, which could provide essential information for the construction of terminal actinide nitride multiple bonds.

In the present work, based on the first isolated L-U-N compound containing the terminal U≡N triple bond (Scheme 1), we have investigated the conformations, electronic states, natural bond orbital (NBO), and electron density of L-An-N species (An = Pa to Pu) with scalar relativistic density functional theory. The oxidation state of uranium in neutral and anionic L-U-N compounds is hexavalent and pentavalent, respectively. Here we change construction to explore a series of new actinide compounds by replacing U in L-U-N compounds with actinide elements from Pa to Pu. To the best of our knowledge, the comparative bonding studies of molecular compounds across actinide series are limited.[20,32,33,35] Therefore, establishing bonding trends and differences across the early 5f series could provide a more detailed comprehension of basic bonding principles and help obtain chemical knowledge for nuclear fuel cycle applications.

2. COMPUTATIONAL DETAILS

The geometry optimizations were carried out using the DFT method with the Gaussian09 program.[36] To test the reliability of different DFT methods for our studied molecules, we applied B3LYP,[37,38] BP86,[39] PBE,[40] and M06-2X[41] methods for the neutral and anionic L-U-N species. According to the relative errors of bond lengths and vibrational frequencies, the BP86 functional is in surprisingly better agreement with experimental results as mentioned below, which is also a widely used functional for actinides.[42,43] Therefore, all actinide species in this work have been optimized with the BP86 method. The quasi-relativistic small-core pseudopotential ECP60MWB along with the corresponding ECP60MWB-SEG valence basis sets were applied for actinide atoms (An = Pa to Pu).[44−46] For the other atoms (H, C, N, and Si), the 6-31G(d) basis set was used. The quasi-relativistic small-core pseudopotential replaces 60 core electrons for actinide atoms, whereas the remaining electrons were represented by the associated valence basis set. A small-core ECP is generally considered to be more accurate than a large-core ECP. Spin−orbit effects were neglected in this work. It should be pointed out that spin−orbital effects should be small, but it does have a potential effect on geometries and vibrational frequencies. The unrestricted Kohn−Sham formalism was performed for all L-An-N species with unpaired 5f electrons, and the different spin states (singlet, doublet, triplet, and quartet) for all species were also considered, and spin contamination was found to be small as mentioned below. According to the total electronic energies of all species with different spin states, the highest spin state was confirmed to be the ground state. Harmonic vibrational frequencies obtained analytically at the optimized structures are all positive values. Natural population analysis (NPA) was carried out using the NBO method with NBO 5.0 program[47] as implemented in the Amsterdam density functional (ADF 2010.02) package.[48,49] Strictly speaking, the density matrices are required to perform NBO analysis. Although the DFT method can only provide density functions, it has also been proven to obtain reasonable results of bonding nature.[18,32,50] In NBO calculations, the BP86 method and the Slater type orbital (STO) basis set with the quality of triple-ζ plus polarization (TZP) basis set were used,[51] without the frozen core. The scalar relativistic (SR) effects were taken into account using the zero-order regular approximation (ZORA) approach.[52] Additionally, the topological analysis of the electron density for the terminal multiple An−N1 bond were performed by employing quantum theory of atoms in molecules (QTAIM) with ADF program and Multiwfn code,[53] respectively.

3. RESULTS AND DISCUSSION

3.1. Optimized Geometries and Harmonic Vibrational Frequencies. To date, there are several benchmarks for the DFT methods for studying actinide complexes. Averkiev et al. have done extensive studies on the bond energies and ionization potentials of actinide compounds using various DFT functionals and found that the B3LYP method gives more accurate results.[38] Vetere et al. have also systematically performed on comparative studies of quasi-relativistic DFT (pure and hybrid) methods for the bonding of trivalent lanthanide and actinide complexes and pointed out that the pure DFT (BP86 and PBE) functionals give more reliable results compared to hybrid methods.[42] Therefore, to calibrate the reliability of theoretical methods for the compounds studied here, four exchange-correlation functionals, B3LYP, BP86, PBE, and M06-2X were selected. Table 1 lists the terminal U−N1 bond lengths and their harmonic vibrational frequencies in neutral and anionic L-U-N species using four functionals with 6-31G(d) basis set, respectively. The relative errors with the BP86 level of theory are the smallest among these four functionals. For example, the relative errors of the U−N1 bond length and the corresponding stretching vibrational frequency in the anionic L-U-N compound are only 1.1% and 2.0% with the BP86 functional, respectively. In addition, to make clear the effect of the diffuse function, we have also carried out the

dx.doi.org/10.1021/ic501006p | Inorg. Chem. 2014, 53, 9607−9614

Table 2. Selected An−N Bond Distances (Å), Bond Angles (deg), and Harmonic Vibrational Frequencies in L-An-N Species at BP86 Level of Theory

L−An−N[a]	An−N1	An−N2	An−N3	An−N4	An−N5	N5AnN1	N3AnN4	N3AnN2	N4AnN2	νs(An−N1)
Pa(−1,1)	1.825	2.430	2.410	2.412	2.756	177.90	107.21	109.43	107.71	927
U(−1,2)	1.805	2.403	2.389	2.392	2.740	177.15	107.11	109.52	106.83	917
Np(−1,3)	1.791	2.389	2.411	2.396	2.631	177.42	110.01	109.63	108.47	871
Pu(−1,4)	1.791	2.393	2.390	2.407	2.606	170.48	109.53	110.22	109.64	773
U(0,1)	1.773	2.291	2.295	2.300	2.643	177.35	109.06	108.13	108.03	938
Np(0,2)	1.761	2.304	2.299	2.274	2.564	152.84	108.23	110.70	104.73	894
Pu(0,3)	1.758	2.249	2.303	2.289	2.700	146.67	109.17	111.13	103.53	830

[a]The values in parentheses are the molecular charge and the most stable spin state, respectively.

geometrical optimizations and frequency calculations using the 6-31+G(d) basis set. It can be clearly seen that the bond lengths are the same with those obtained with the 6-31G(d) basis set (Table 1), and the relative errors of the harmonic vibrational frequencies decrease a little bit compared to 6-31G(d) basis set. Therefore, based on our comparisons of the structures and frequencies using four functionals, the following optimizations, vibrational frequencies and NBO analysis of the L-An-N species were applied using the BP86 method with the 6-31G(d) basis set in this work.

Here we selected actinide elements from Pa to Pu to replace U in L-U-N compounds, so that a series of new actinide compounds change construction to explore at the molecular level. The oxidation states of actinide elements studied here are hexavalent and pentavalent in neutral and anionic L-An-N (An = Pa−Pu) species, respectively. We have optimized a series of actinide species, L-An-N (An = Pa−Pu), in neutral and anionic states at the BP86 level of theory. Because 5f orbital hosts the unpaired electrons, the stabilities of these compounds at different electronic spin states were considered. The corresponding highest spin state was confirmed to be the ground state according to the obtained total electronic energies of each actinide species as listed Table S1 of Supporting Information (SI). The spin contamination of the ground state was found to be small except for those of L-Pu-N complexes (Table S2 of SI), and the largest deviation from the ideal value is 0.21 for the quartet state L-Pu-N, which suggests the multireference character. Table 2 lists the predicted An−N bond distances and the An-N1 vibrational frequencies in neutral and anionic L-An-N species at the BP86//ECP60MWB-SEG/6-31G(d) level of theory. To determine the trend in five An−N bonds with increasing atomic number of actinide, the bond distances of An−N1(terminal nitrogen) and An−N5 (amido nitrogen), and the average An−N bond distances with nitrogen atom from imido group (N_{imido} = N2, N3, and N4) are plotted in Figure 1.

It can be clearly seen from Figure 1 that the terminal An−N1 bond distances in neutral and anionic L-An-N species both decrease gradually from Pa to Np, in accordance with the actinide contraction. For example, in anionic species, the An−N1 bond distance shortens by 0.034 Å from L−Pa−N (1.825 Å) to L−Pu−N (1.791 Å). The trend of the An−N1 bond distances in L-An-N compounds is consistent with the ionic radii of actinides(V).[54] Furthermore, the terminal An−N1 bond distances in neutral L-An-N species are shorter compared to those in the corresponding anionic compounds, which reveal that the strength of the An−N1 bond in neutral species is stronger than that in the corresponding anionic one. Similar to the terminal An−N1 bond, the average bond distances of three An−N_{imido} bonds (N_{imido} = N_2, N_3, and N_4) in neutral and anionic L-An-N species also decrease from U to Pu, and the

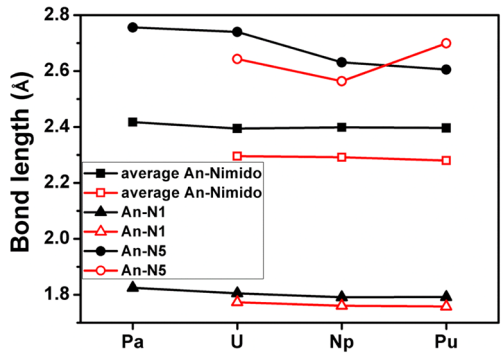

Figure 1. Bond distances of terminal An−N1 (triangle) and An−N5 (circle) as well as the average bond distances of An−N_{imido} (square) in neutral (red line) and anionic (black line) L-An-N species (An = Pa−Pu) at the BP86 level of theory.

average distance of three An−N_{imido} bonds in neutral L-An-N species is shorter than that in the corresponding anionic species. The bond distances between actinide atoms and nitrogen atoms of amine (An−N5) are the longest among all An−N bonds. For instance, the bond length of U−N5 in neutral L-U-N compound (2.643 Å) is 0.910 Å longer than that of the terminal U−N1 (2.733 Å). However, unlike terminal An−N1 and An−N_{imido} bonds, the bond length change of An-N5 with the atomic number is irregular. Additionally, the bond angles of N5AnN1 (Table 2) in all anionic L-An-N species are close to 180° except that of N5PuN1 with a deviation of 10°. However, in the neutral species, only the bond angle of N5UN1 still remains about 180°. We also provide the harmonic vibrational frequencies of the An−N1 bonds at the BP86 level of theory in Table 2. The An-N1 harmonic vibrational frequency in neutral and anionic L-An-N species decreases with increasing atomic number of actinide. Moreover, the harmonic vibrational frequency of the An−N1 bond in neutral L-An-N species is larger than that in the corresponding anionic one, which reflects the trend of the An−N1 bond in neutral and anionic species across the actinide series.

3.2. Molecular Orbitals. To further study the bonding character between actinide (An = Pa−Pu) and the terminal nitrogen, the canonical valence molecular orbitals (MOs) involved in the An−N1 bond are shown in Figures S1−S2, Supporting Information. The MO diagrams and the corresponding orbital energy levels for all L-An-N species are displayed in Figure 2. It can be clearly seen that these MOs mainly possess σ and π character. The energy level of σ MOs for all compounds decreases with increasing atomic number of actinide, and π MOs follow the same trend. Taking the σ MO in anionic L-An-N species as an example, the order of energy is Pa(−0.824 eV) > U(−1.332 eV) > Np(−1.478 eV) >

dx.doi.org/10.1021/ic501006p | Inorg. Chem. 2014, 53, 9607−9614

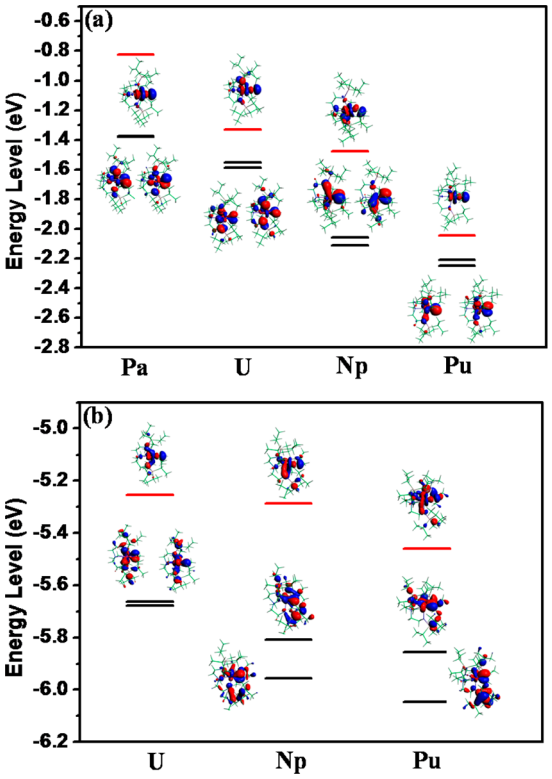

Figure 2. Energy levels of alpha-spin MOs between actinide and terminal nitrogen atom (N1) in (a) anionic and (b) neutral L-An-N species. The red and black lines denote the energy levels of σ and π MOs, respectively. The isosurface value of the MOs is set to be 0.03 au.

Pu(−2.043 eV). Moreover, the energy level of the σ MO is higher than those of π MOs for all L-An-N species. In addition, the energies of the MOs for all neutral L-An-N species are much lower than those of corresponding anionic compounds because an electron is removed from the anionic species. According to the energies of the An-N1MOs, the terminal An-N1 multiple bond in neural L-An-N species is stronger compared to those in the corresponding anionic ones. This is consistent with the result from the An−N1 bond as discussed above.

3.3. NBO Analysis. We also performed the natural bond orbital (NBO) analysis at the BP86/TZP level of theory using NBO program built in ADF suit. The natural charges on the actinide and nitrogen atoms in L-An-N species are displayed in Figure 3, and the charge values are also provided in Table S3 of Supporting Information. For neutral and anionic species, with increasing atomic number of actinide, the natural charges (i) on the actinide atom decrease; (ii) on the terminal nitrogen (N1) increase; (iii) on the nitrogen atom of imido (N2, N3, and N4) and amido (N5) groups are almost similar. These results indicate that the An−N (N = N2−N5) bonds possess similar bonding character across the actinide series, whereas the terminal An−N1 bond obviously changes. In addition, based on the natural charges obtained here, the Pa atom possesses the largest positive charge and the N1 atoms possesses the largest negative charge in L-Pa-N species, suggesting the strongest interaction between Pa and terminal N1 atoms among all the L-An-N species.

The electronic configurations of the isolated actinide atoms are as below: Pa, $[Rn]7s^2 5f^2 6d^1$; U, $[Rn]7s^2 5f^3 6d^1$; Np, $[Rn]7s^2 5f^4 6d^1$; and Pu, $[Rn]7s^2 5f^6$. The natural electronic configurations of actinide and terminal N1 atoms in neutral and anionic L-An-N species are provided in Table 3. It can be found that the natural electronic configurations of actinide are similar for neutral and anionic species. It is clearly observed that for the actinide atom: (i) the electrons mostly occupy 5f shell, and the remaining electrons residue 6d and 7s shells, indicating that the 5f orbital is mainly involved in the An−N1 bond. It can be concluded that the 5f orbital may be more suitable to multiple bonding than the 6d orbital due to its more favorable angular variation and energies; (ii) 5f population occupancies increase with increasing actinide atomic number, whereas 6d and 7s occupancies decrease, also denoting that more 5f orbital component participates in bonding across the actinide series. As for the terminal N_1 atom: (i) the electrons residue 2s and 2p shells, the occupation numbers of 2p shell decrease and those of 2s shell increase with increasing actinide atomic number; (ii)

Table 3. Natural Electronic Configurations of Actinide and Terminal Nitrogen Atoms (N1) in Neutral and Anionic L-An-N Species

species	An	N1
Pa(−1,1)[a]	$[Rn]7s^{0.19}5f^{1.53}6d^{0.55}7p^{0.02}8s^{0.01}$	$[He]2s^{1.91}2p^{4.44}3d^{0.03}$
U(−1,2)	$[Rn]7s^{0.21}5f^{2.91}6d^{0.49}7p^{0.02}8s^{0.01}$	$[He]2s^{1.90}2p^{4.25}3d^{0.02}$
Np(−1,3)	$[Rn]7s^{0.19}5f^{4.16}6d^{0.44}7p^{0.02}8s^{0.01}$	$[He]2s^{1.91}2p^{4.09}3d^{0.02}$
Pu(−1,4)	$[Rn]7s^{0.19}5f^{5.32}6d^{0.38}7p^{0.02}8s^{0.01}$	$[He]2s^{1.92}2p^{3.95}3d^{0.01}$
U(0,1)	$[Rn]7s^{0.17}5f^{2.77}6d^{0.50}7p^{0.02}8s^{0.01}$	$[He]2s^{1.90}2p^{4.05}3d^{0.03}$
Np(0,2)	$[Rn]7s^{0.17}5f^{4.25}6d^{0.46}7p^{0.02}8s^{0.01}$	$[He]2s^{1.90}2p^{3.87}\ 3d^{0.02}$
Pu(0,3)	$[Rn]7s^{0.16}5f^{5.41}6d^{0.42}7p^{\ 0.02}8s^{0.01}$	$[He]2s^{1.90}2p^{3.77}3d^{0.01}$

[a]The values in parentheses are the molecular charges and the most stable spin state, respectively.

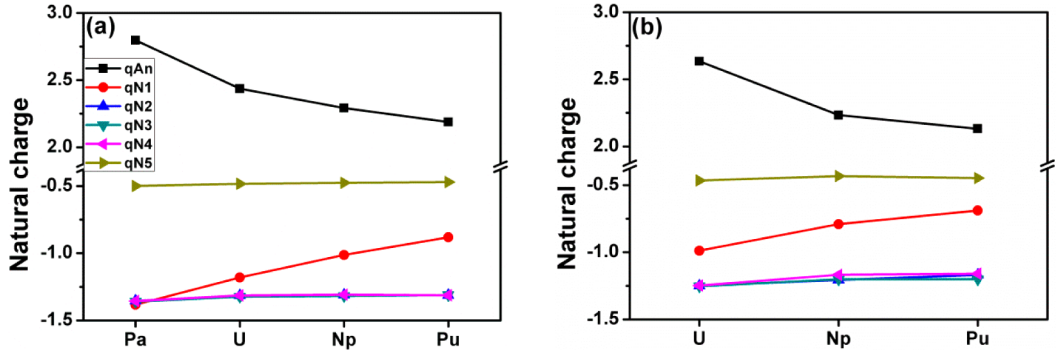

Figure 3. Natural charges on the actinide and nitrogen atoms in (a) anionic and (b) neutral L-An-N species.

dx.doi.org/10.1021/ic501006p | Inorg. Chem. 2014, 53, 9607−9614

the occupation numbers of 2p shell is less in neutral L-An-N species than in corresponding anionic states. Additionally, the electronic configuration of the isolated nitrogen atom is $[He]2s^2 2p^3$, the occupation numbers on N 2s shell in L-An-N species decrease about 0.1, and those on 2p shell show larger increase in the range of 1.0−1.5. These results suggest that the redundant electrons on N 2p shell come from the N 2s shell and related shells in the actinide atom.

Bond order is a measurement of bond multiplicities and is related to bond strength and relative stability in similar bonding situation. Table 4 lists the obtained Mayer bonds orders of the

Table 4. Mayer Bond Order of An−N Bonds in Neutral and Anionic L-An-N Species

species	An−N1	An−N2	An−N3	An−N4	An−N5
Pa(−1,1)	2.943	0.659	0.634	0.651	0.276
U(−1,2)	2.935	0.654	0.628	0.638	0.302
Np(−1,3)	2.948	0.654	0.642	0.628	0.354
Pu(−1,4)	2.895	0.633	0.626	0.600	0.331
U(0,1)	2.965	0.877	0.863	0.866	0.397
Np(0,2)	2.935	0.887	0.881	0.899	0.385
Pu(0,3)	2.845	0.875	0.848	0.877	0.308

An−N bond in neutral and anionic L-An-N species at the BP86/TZP level of theory. It is clearly seen that the An−N1 bond order decreases with increasing atomic number for neutral and anionic L-An-N species except for the anionic L-Np-N compound. Furthermore, the bond orders of An−N1 are over 2.85, suggesting that the An−N1 bonds have obvious triple bond character. The bond orders of An−N5 in all L-An-N compounds range from 0.28 to 0.40, which shows that the An−N5 bond possesses minor covalent character and the electrostatic interactions play a dominant role. As for three An−N_{imido} bonds, the values are in the range of 0.60−0.66 and 0.85−0.90 for anionic and neutral L-An-N species, respectively. This denotes that the three An−N_{imido} bonds are single bonds and possess covalent character. In addition, the An−N1 bond order in anionic L-An-N species is somewhat larger than that in the corresponding neutral ones, except for L-U-N compounds. The U−N1 bond order is 2.935 in the anionic L-U-N compound, whereas it reaches to 2.965 in the neutral L-U-N compound.

To obtain more bonding details on the terminal multiple An−N1 bonds, localized NBO analysis was also performed. The natural localized molecular orbitals of An−N1 are distinct σ and π bonds as displayed in Figures S3−S4, Supporting Information. The calculated compositions of An−N1 bonds and the contribution of each atomic orbital for neutral and anionic species are listed in Tables S3−S5, Supporting Information. In order to clearly compare the trend of actinide participation in bonding, Figure 4 provides the percentage of actinide atoms in terminal multiple An−N1 bonds. It is important to point out that the actinide percentage in terminal An-N1 bonds increase with increasing actinide atomic number in neutral and anionic L-An-N species. Taking anionic L-Pa-N and L-Pu-N compounds as examples, the Pa−N1 π bonds contain about 21% Pa and 79% N character, while the Pu−N1 π bonds contain about 42% Pu and 58% N character. Furthermore, the percentage of actinide in An−N1 π bond is somewhat larger in neutral L-An-N species compared to the corresponding values in anionic ones. In addition, these π orbitals mainly originate from actinide 6d and 5f orbitals ($5f_\phi$ atomic orbital) and N1 2p orbital. As shown in Figure 5, the bonding contribution from 5f orbital increases and that from

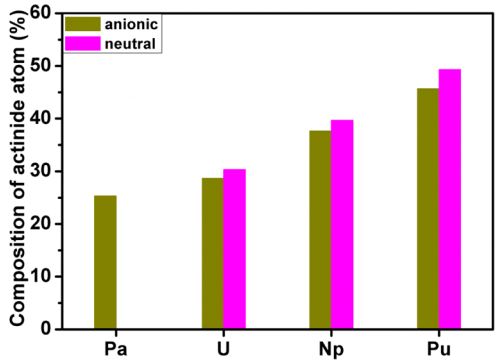

Figure 4. Average percentage of actinide atom in the terminal multiple An−N1 bond for the neutral and anionic L-An-N species.

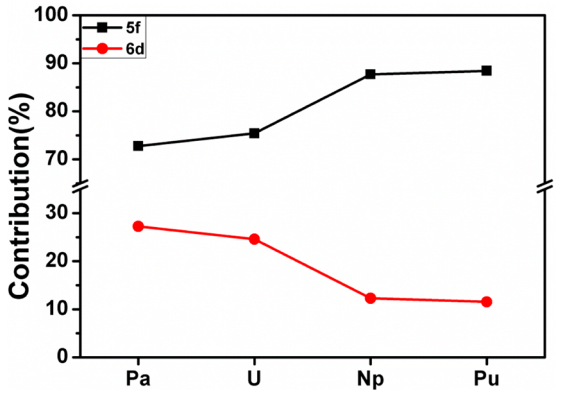

Figure 5. Average contributions of actinide 5f and 6d orbitals to two π orbitals of an An−N bond in the anionic L-An-N species.

the 6d orbital decreases when An changes from Pa to Pu. Taking π orbitals in anionic L-U-N and L-Pu-N species as an example, the 5f orbital component is about 73% for U and increases to about 88% for Pu. These results suggest that the actinide percentage as well as their 5f orbital contribution to the An−N1 multiple bonding both increase with increasing actinide atomic number, which is in good agreement with their electronic configuration results. As for the An-N1 σ orbital, the N1 is composed of 2p orbital as well as a little bit of 2s orbital. The actinide atom is composed of all the 7s, 6p, 6d, and 5f ($5f_\sigma$ atomic orbital) contributions. As provided in Table S3, Supporting Information, the U−N1 σ orbital in neutral complex contains about 69% N1 and 31% U character. The N component includes 7% 2s and 92% 2p orbitals, and the U component is composed of 2% 7s, 3% 6p, 49% 6d, and 46% 5f orbitals. These results give a hint that the contributions of the 5f orbital for forming terminal multiple An−N1 bond increase with increasing actinide atomic number.

3.4. Topological Analysis. The topological analysis of the electron density of the An−N1 bond has also been performed by employing QTAIM with ADF and Multiwfn code, respectively. This method has been used for actinide compounds and could provide good trends with the strength of chemical bonds.[27,33,55,56] A bond critical point (BCP) is the (3, −1) saddle point on electron density $[\rho(r)]$ curvature being a minimum in the direction of the atomic interaction line and a maximum in the two directions perpendicular to it.[57] Within

dx.doi.org/10.1021/ic501006p | Inorg. Chem. 2014, 53, 9607−9614

QTAIM, a chemical bond is defined by the presence of a line of maximum $\rho(r)$ along a bond path between two atoms and BCP. Therefore, the topological analysis of electron density could provide valuable information about the properties of the bond.[58,59]

Here, we focused on the $\rho(r)$, its Laplacian $[\nabla^2\rho(r)]$ and the total electronic energy density $[H(r)]$ (the sum of the kinetic and potential energy densities) at the An-N1 BCP in Table 5.

Table 5. Electron Density $[\rho(r)$, au$]$, Its Laplacian $[\nabla^2\rho(r)$, au$]$, and the Total Electronic Energy Density $[H(r)$, au$]$ at Terminal An−N1 Bond Critical Point in L-An-N Species

species	$\rho(r)^a$	$\nabla^2\rho(r)^a$	$\rho(r)^b$	$H(r)^b$
Pa(−1,1)	0.294	−0.014	0.300	−0.286
U(−1,2)	0.304	−0.010	0.309	−0.291
Np(−1,3)	0.305	−0.013	0.310	−0.284
Pu(−1,4)	0.295	−0.019	0.298	−0.260
U(0,1)	0.325	−0.018	0.332	−0.329
Np(0,2)	0.325	−0.012	0.331	−0.319
Pu(0,3)	0.316	−0.017	0.321	−0.297

[a]The values obtained with ADF program. [b]The values obtained with Multiwfn program.

In general, the electron density at BCP $\rho(r) > 0.20$ au and $\nabla^2\rho(r) < 0$ describe a covalent bond, while $\rho(r) < 0.10$ au and $\nabla^2\rho(r) > 0$ is for an ionic bond. $H(r)$ at the BCP is negative for interactions with significant sharing of electrons and its magnitude can reflect the covalence of the bonding interaction.[60] There have been several previous works reports on covalency in actinide compounds using QTAIM topological analysis. For example, Tassell et al. reported that very little covalency exists in An−Cp bonding of $AnCp_4$ (Cp = η^5-C_5H_5, An = Th-*Cm*) compounds with QTAIM topological analysis.[33,61] Very recently, the covalency of An−C bond in a series of actinocenes (An = Th-*Cm*) has been studied with topological analysis of electron density via the QTAIM approach.[35] Their result show that the values of $\rho(r)$ at actinide-carbon BCP are about 0.04 a.u corresponding to a positive Laplacian, which indicates that the ionic interaction predominate the actinide-carbon bonds. In recent work of Minasian et al., the new evidence for 5f covalency in thorocene and uranocene was first determined from carbon K-edge X-ray absorption spectra.[62] Both the experimental and theoretical results showed that the covalency does not increase uniformly for different molecular orbital interactions with later actinides.[62] In this work, the calculated $\rho(r)$ at An-N1 BCP has been obtained using ADF and Multiwfn programs. As shown in Table 5, $\rho(r)$ with ADF program are only about 0.005 au smaller than the corresponding values from Multiwfn program, and the trend of $\rho(r)$ with the two programs has strong similarity. For all L-An-N species, the $\rho(r)$ at An-N1 BCP are over 0.29 au and $\nabla^2\rho(r)$ are negative, which show that the terminal An−N1 multiple bond possesses covalent character. The negative $H(r)$ at An-N1 BCP also indicates that the terminal An−N1 multiple bond exhibits more covalent interaction. Moreover, the magnitude of $H(r)$ at An−N1 BCP decreases from U to Pu for neutral and anionic species, which reflects that the covalent interaction between actinide and nitrogen atom decreases. In addition, the $H(r)$ at An-N1 BCP in neutral L-An-N species is larger than that in the corresponding anionic compounds. This result suggests that the terminal multiple An-N1 appear to be more covalent for neutral L-An-N species than the corresponding anionic ones.

According to the topological and NBO analyses, the proportion of covalent character in the terminal An−N1 bond decreases from An = U to Pu. The contribution of 5f orbital increases and that of 6d orbital decreases in participating in the terminal An−N1 bond with increasing atomic number. It is worthwhile to point out that the contributions of 6d orbital to covalency are larger in magnitude than 5f orbital. In addition, the contribution of 5f orbital is mainly ϕ-type orbital, and therefore, the covalency decreases for $5f_\phi$ orbital across the actinide series.

3.5. Electron Affinity. The electron affinity (EA) of a neutral molecule is the binding energy of an electron to the neutral molecule. EA is calculated by the difference of the total electronic energies (E) between neutral molecule and their anionic forms. Thus, the EA is defined as

$$\mathrm{EA} = E^{\mathrm{neutral}} - E^{\mathrm{anion}} \quad (3)$$

Here we calculated the adiabatic EA; that is, the total electronic energies come from their optimized geometries.

Table 6 shows that the predicted adiabatic EA values of the neutral L-An-N species are all positive, which indicates that the neutral L-An-N species are less stable compared to their anionic analogues in the gas phase. Though the neutral L-U-N compound has been experimentally isolated, it easily converts into new complex especially at the condition of sunlight irradiation.[15] Our predicted EA of neutral L-U-N compound is in good agreement with the experimental results.[15]

Table 6. Adiabatic EA (eV) of Neutral L-An-N Species at the BP86 Level of Theory

species	L-U-N	L-Np-N	L-Pu-N
EA	1.104	1.635	2.054

4. CONCLUSIONS

In summary, the ground state geometric and electronic structures of a series of L-An-N (An = Pa−Pu) species were investigated using the scalar relativistic DFT method. The BP86 functional was confirmed to be a more reliable method to deal with geometries and harmonic vibrational frequencies of L-An-N species by comparison with experimental data. The bond lengths of the terminal An−N1 multiple bonds gradually decrease from An = Pa to Pu, in accord with the actinide contraction. The terminal multiple An−N1 bonds contain one σ and two π molecular orbitals, and their energy levels decrease from An = Pa to Pu. The Mayer bond orders of terminal An−N1 bond decrease across the actinide series, indicating that the strength of An−N1 bond becomes weaker with increasing atomic number. The electronic configurations and the NBO analysis show that the electrons mostly occupy 5f shell for actinide atoms, and the population occupancies and contributions of 5f orbital gradually grow for the terminal An−N1 bonds from An = Pa to Pu. By contrast, the contributions of the 6d orbital to the multiple An−N1 bonds were found decrease across the actinide series. The topological analysis of the electron density shows that the terminal An−N1 multiple bond exhibits more covalent interaction. Moreover, the magnitude of $H(r)$ at An-N1 BCP reflects that the covalent interaction between actinide and the terminal nitrogen atom decreases from An = U to Pu. That is to say, the 6d orbital contributes to

dx.doi.org/10.1021/ic501006p | Inorg. Chem. 2014, 53, 9607−9614

covalency to a larger extent than the 5f orbital. In addition, electron affinities of all neutral L-An-N species are positive, revealing that the neural states are unstable in the gas phase. This work might help to understand the electronic structure characteristics of actinide compounds and establish a more detailed understanding of electronic structure changes and basic bonding trends across the actinide series. Furthermore, this work could shed light on the potential implications for actinides including nuclear fuel cycle applications and environmental remediation.

■ ASSOCIATED CONTENT

Supporting Information

The alpha-spin molecular orbital diagrams between actinide and terminal nitrogen atoms and their corresponding energies, natural bond orbital, total electronic energies, spin contamination, NPA charges, and NBO analysis. This material is available free of charge via the Internet at http://pubs.acs.org.

■ AUTHOR INFORMATION

Corresponding Authors

*(W.-Q.S.) E-mail: shiwq@ihep.ac.cn.
*(Z.-F.C.) E-mail: zfchai@suda.edu.cn.

Notes

The authors declare no competing financial interest.

■ ACKNOWLEDGMENTS

This work was supported by the National Natural Science Foundation of China (Grant Nos. 91326202, 11205169, 21101157, 21261140335, 91126006, 21477130), the "Strategic Priority Research Program" of the Chinese Academy of Sciences (Grant No. XDA030104), and China Postdoctoral Science Foundation funded project (Grant No. 2013T60173). The results described in this work were obtained on the ScGrid of Supercomputing Center, Computer Network Information Center of Chinese Academy of Sciences.

■ REFERENCES

(1) Cotton, F. A.; Curtis, N. F.; Harris, C. B.; Johnson, B. F. G.; Lippard, S. J.; Mague, J. T.; Robinson, W. R.; Wood, J. S. *Science* **1964**, *145*, 1305−1307.
(2) Cotton, F. A. *Chem. Soc. Rev.* **1975**, *4*, 27−53.
(3) Nguyen, T.; Sutton, A. D.; Brynda, M.; Fettinger, J. C.; Long, G. J.; Power, P. P. *Science* **2005**, *310*, 844−847.
(4) Clouston, L. J.; Siedschlag, R. B.; Rudd, P. A.; Planas, N.; Hu, S.; Miller, A. D.; Gagliardi, L.; Lu, C. C. *J. Am. Chem. Soc.* **2013**, *135*, 13142−13148.
(5) Cramer, R. E.; Maynard, R. B.; Paw, J. C.; Gilje, J. W. *J. Am. Chem. Soc.* **1981**, *103*, 3589−3590.
(6) Brown, D. R.; Denning, R. G. *Inorg. Chem.* **1996**, *35*, 6158−6163.
(7) Burns, C. J. *Science* **2005**, *309*, 1823−1824.
(8) Andrews, L.; Wang, X.; Lindh, R.; Roos, B. O.; Marsden, C. J. *Angew. Chem., Int. Ed.* **2008**, *47*, 5366−5370.
(9) Cantat, T.; Arliguie, T.; Noël, A.; Thuéry, P.; Ephritikhine, M.; Floch, P. L.; Mézailles, N. *J. Am. Chem. Soc.* **2009**, *131*, 963−972.
(10) Fox, A. R.; Cummins, C. C. *J. Am. Chem. Soc.* **2009**, *131*, 5716−5717.
(11) Hayton, T. W. *Dalton Trans.* **2010**, *39*, 1145−1158.
(12) Ma, G.; Ferguson, M. J.; McDonald, R.; Cavell, R. G. *Inorg. Chem.* **2011**, *50*, 6500−6508.
(13) King, D. M.; Tuna, F.; McInnes, E. J. L.; McMaster, J.; Lewis, W.; Blake, A. J.; Liddle, S. T. *Science* **2012**, *337*, 717−720.
(14) Camp, C.; Pécaut, J.; Mazzanti, M. *J. Am. Chem. Soc.* **2013**, *135*, 12101−12111.
(15) King, D. M.; Tuna, F.; McInnes, E. J. L.; McMaster, J.; Lewis, W.; Blake, A. J.; Liddle, S. T. *Nat. Chem.* **2013**, *5*, 482−488.
(16) Smiles, D. E.; Wu, G.; Hayton, T. W. *J. Am. Chem. Soc.* **2013**, *136*, 96−99.
(17) Zhou, M.; Andrews, L.; Li, J.; Bursten, B. E. *J. Am. Chem. Soc.* **1999**, *121*, 9712−9721.
(18) Hu, H.-S.; Qiu, Y.-H.; Xiong, X.-G.; Schwarz, W. H. E.; Li, J. *Chem. Sci.* **2012**, *3*, 2786−2796.
(19) Kraft, S. J.; Walensky, J.; Fanwick, P. E.; Hall, M. B.; Bart, S. C. *Inorg. Chem.* **2010**, *49*, 7620−7622.
(20) Li, J.; Bursten, B. E. *J. Am. Chem. Soc.* **1997**, *119*, 9021−9032.
(21) Kaltsoyannis, N. *Chem. Soc. Rev.* **2003**, *32*, 9−16.
(22) Roos, B. O.; Malmqvist, P.-Å.; Gagliardi, L. *J. Am. Chem. Soc.* **2006**, *128*, 17000−17006.
(23) Vallet, V.; Macak, P.; Wahlgren, U.; Grenthe, I. *Theor. Chem. Acc.* **2006**, *115*, 145−160.
(24) Hagberg, D.; Bednarz, E.; Edelstein, N. M.; Gagliardi, L. *J. Am. Chem. Soc.* **2007**, *129*, 14136−14137.
(25) Schreckenbach, G.; Shamov, G. A. *Acc. Chem. Res.* **2009**, *43*, 19−29.
(26) Lan, J.-H.; Shi, W.-Q.; Yuan, L.-Y.; Zhao, Y.-L.; Li, J.; Chai, Z.-F. *Inorg. Chem.* **2011**, *50*, 9230−9237.
(27) Vlaisavljevich, B.; Miró, P.; Cramer, C. J.; Gagliardi, L.; Infante, I.; Liddle, S. T. *Chem.—Eur. J.* **2011**, *17*, 8424−8433.
(28) Wang, D.; van Gunsteren, W. F.; Chai, Z. *Chem. Soc. Rev.* **2012**, *41*, 5836−5865.
(29) Wang, C.-Z.; Lan, J.-H.; Zhao, Y.-L.; Chai, Z.-F.; Wei, Y.-Z.; Shi, W.-Q. *Inorg. Chem.* **2013**, *52*, 196−203.
(30) Hu, H.-S.; Wei, F.; Wang, X.; Andrews, L.; Li, J. *J. Am. Chem. Soc.* **2014**, *136*, 1427−1437.
(31) Wu, Q.-Y.; Lan, J.-H.; Wang, C.-Z.; Xiao, C.-L.; Zhao, Y.-L.; Wei, Y.-Z.; Chai, Z.-F.; Shi, W.-Q. *J. Phys. Chem. A* **2014**, *118*, 2149−2158.
(32) Zhou, J.; Sonnenberg, J. L.; Schlegel, H. B. *Inorg. Chem.* **2010**, *49*, 6545−6551.
(33) Kaltsoyannis, N. *Inorg. Chem.* **2013**, *52*, 3407−3413.
(34) Lukens, W. W.; Edelstein, N. M.; Magnani, N.; Hayton, T. W.; Fortier, S.; Seaman, L. A. *J. Am. Chem. Soc.* **2013**, *135*, 10742−10754.
(35) Kerridge, A. *RSC Adv.* **2014**, *4*, 12078−12086.
(36) Frisch, M. J.; Trucks, G. W.; Schlegel, H. B.; Scuseria, G. E.; Robb, M. A.; Cheeseman, J. R.; Scalmani, G.; Barone, V.; Mennucci, B.; Petersson, G. A.; Nakatsuji, H.; Caricato, M.; Li, X.; Hratchian, H. P.; Izmaylov, A. F.; Bloino, J.; Zheng, G.; Sonnenberg, J. L.; Hada, M.; Ehara, M.; Toyota, K.; Fukuda, R.; Hasegawa, J.; Ishida, M.; Nakajima, T.; Honda, Y.; Kitao, O.; Nakai, H.; Vreven, T.; Montgomery, Jr., J. A.; Peralta, J. E.; Ogliaro, F.; Bearpark, M.; Heyd, J. J.; Brothers, E.; Kudin, K. N.; Staroverov, V. N.; Kobayashi, R.; Normand, J.; Raghavachari, K.; Rendell, A.; Burant, J. C.; Iyengar, S. S.; Tomasi, J.; Cossi, M.; Rega, N.; Millam, N. J.; Klene, M.; Knox, J. E.; Cross, J. B.; Bakken, V.; Adamo, C.; Jaramillo, J.; Gomperts, R.; Stratmann, R. E.; Yazyev, O.; Austin, A. J.; Cammi, R.; Pomelli, C.; Ochterski, J. W.; Martin, R. L.; Morokuma, K.; Zakrzewski, V. G.; Voth, G. A.; Salvador, P.; Dannenberg, J. J.; Dapprich, S.; Daniels, A. D.; Farkas, Ö.; Foresman, J. B.; Ortiz, J. V.; Cioslowski, J.; Fox, D. J. *Gaussian09*; Gaussian, Inc.: Wallingford, CT, 2009.
(37) Lee, C. T.; Yang, W. T.; Parr, R. G. *Phys. Rev. B* **1988**, *37*, 785−789.
(38) Averkiev, B.; Mantina, M.; Valero, R.; Infante, I.; Kovacs, A.; Truhlar, D.; Gagliardi, L. *Theor. Chem. Acc.* **2011**, *129*, 657−666.
(39) Perdew, J. P. *Phys. Rev. B* **1986**, *33*, 8822.
(40) Adamo, C.; Barone, V. *J. Chem. Phys.* **1999**, *110*, 6158−6170.
(41) Zhao, Y.; Truhlar, D. *Theor. Chem. Acc.* **2008**, *120*, 215−241.
(42) Vetere, V.; Maldivi, P.; Adamo, C. *J. Comput. Chem.* **2003**, *24*, 850−858.
(43) Austin, J. P.; Sundararajan, M.; Vincent, M. A.; Hillier, I. H. *Dalton Trans.* **2009**, 5902−5909.
(44) Küchle, W.; Dolg, M.; Stoll, H.; Preuss, H. *J. Chem. Phys.* **1994**, *100*, 7535−7542.
(45) Cao, X.; Dolg, M.; Stoll, H. *J. Chem. Phys.* **2003**, *118*, 487−496.

(46) Cao, X.; Dolg, M. *J. Mol. Struct. (THEOCHEM)* **2004**, *673*, 203−209.
(47) Glendening, E. D.; Badenhoop, J. K.; Reed, A. E.; Carpenter, J. E.; Bohmann, J. A.; Morales, C. M.; Weinhold, F. *NBO 5.0*; Theoretical Chemistry Institute, University of Wisconsin: Madison, 2001; http://www.chem.wisc.edu/∼nbo5.
(48) Fonseca Guerra, C.; Snijders, J. G.; te Velde, G.; Baerends, E. J. *Theor. Chem. Acc.* **1998**, *99*, 391−403.
(49) te Velde, G.; Bickelhaupt, F. M.; Baerends, E. J.; Fonseca Guerra, C.; van Gisbergen, S. J. A.; Snijders, J. G.; Ziegler, T. *J. Comput. Chem.* **2001**, *22*, 931−967.
(50) Lyon, J. T.; Hu, H.-S.; Andrews, L.; Li, J. *Proc. Natl. Acad. Sci. U. S. A.* **2007**, *104*, 18919−18924.
(51) Van Lenthe, E.; Baerends, E. J. *J. Comput. Chem.* **2003**, *24*, 1142−1156.
(52) Lenthe, E. v.; Baerends, E. J.; Snijders, J. G. *J. Chem. Phys.* **1993**, *99*, 4597−4610.
(53) Lu, T.; Chen, F. *J. Comput. Chem.* **2012**, *33*, 580−592.
(54) Greenwood, N. N.; Earnsgaw, A. *Chemistry of the Elements*, 2nd ed.; Reed Educational and Professional Publishing Ltd: Oxford, 1998; pp 1263−1264.
(55) Arnold, P. L.; Turner, Z. R.; Kaltsoyannis, N.; Pelekanaki, P.; Bellabarba, R. M.; Tooze, R. P. *Chem.—Eur. J.* **2010**, *16*, 9623−9629.
(56) Mountain, A. R. E.; Kaltsoyannis, N. *Dalton Trans.* **2013**, *42*, 13477−13486.
(57) Bader, R. F. W. *J. Phys. Chem. A* **2009**, *113*, 10391−10396.
(58) Bader, R. F. W.; Matta, C. F. *Inorg. Chem.* **2001**, *40*, 5603−5611.
(59) Espinosa, E.; Alkorta, I.; Elguero, J.; Molins, E. *J. Chem. Phys.* **2002**, *117*, 5529−5542.
(60) Cremer, D.; Kraka, E. *Angew. Chem., Int. Ed.* **1984**, *23*, 627−628.
(61) Tassell, M. J.; Kaltsoyannis, N. *Dalton Trans.* **2010**, *39*, 6719−6725.
(62) Minasian, S. G.; Keith, J. M.; Batista, E. R.; Boland, K. S.; Clark, D. L.; Kozimor, S. A.; Martin, R. L.; Shuh, D. K.; Tyliszczak, T. *Chem. Sci.* **2014**, *5*, 351−359.